Journal of Applied Polymer Science

Polyaniline-Functionalized Magnetic Nanoparticles for the Removal of Toxic Dye from Wastewater

Triveni Kumar Mahto, Angshuman Ray Chowdhuri, Sumanta Kumar Sahu
Department of Applied Chemistry, Indian School of Mines, Dhanbad 826004, Jharkhand, India
Correspondence to: S. K. Sahu (E-mail: sumantchem@gmail.com)

ABSTRACT: A novel and inexpensive approach was adopted to develop a magnetic nanocomposite for the adsorption of cationic dye from an aqueous solution. This nanocomposite, which was based on a superparamagnetic iron oxide nanocore, was functionalized with a hydrophilic coating of polyaniline (PANI). The nanoparticle size, colloidal stability, surface chemistry, and magnetic properties were studied extensively by transmission electron microscopy, X-ray diffraction, Fourier transform infrared spectroscopy, and vibrating sample magnetometry. The polymeric functionalized magnetic nanocomposite had an average core size of 20–40 nm and a shell size of 6–10 nm. To evaluate the potential of such nanocomposites for dye adsorption, malachite green (MG) was exposed with different operational parameters, such as the pH, temperature, initial concentration of the dye, contact time, and reusability. The rate of the adsorption followed pseudo-second-order kinetics with the adsorption isotherm fit the Langmuir isotherm model well. The maximum adsorption capacity was 240 mg of MG/g of adsorbent. © 2014 Wiley Periodicals, Inc. J. Appl. Polym. Sci. **2014**, *131*, 40840.

KEYWORDS: adsorption; composites; conducting polymers

Received 11 December 2013; accepted 17 March 2014
DOI: 10.1002/app.40840

INTRODUCTION

Industrialization is considered to be the key for the economic development. However, it is also recognized to be the root cause of environmental pollution. Industrial effluents contain many toxic and hazardous pollutants. Dyes are considered one of the most dangerous pollutants generally released from different industries. The presence of dyes in water consumes oxygen and raises biochemical oxygen demand; this consequently damages aquatic life. There are several dyes that are also carcinogenic, and thus, the development of technologies to restrict their discharge and contamination is important. In recent years, physical, chemical, and microbial biodegradation; membrane separation; bioreactors; fungal consortium; and other methods have been common for treating effluents from industries.[1–3] All of these methods have their own limitations; however, in the current scenario, the adsorption of pollutants using ecofriendly materials is considered to be superior to other techniques because of its low cost, simplicity of design, availability, and ability to treat different dyes. In this regard, much attention has recently been paid to nanotechnology.[4–6] Several researchers have synthesized different types of nanoparticles for applications in dye removal.[7–10]

Recently, magnetic nanomaterials have been used as promising adsorbents with a high surface area; they possess magnetic properties to facilitate efficient separation within a short time through the use of an external magnetic field. For example, Mahmoodi et al.[11] synthesized a biocompatible sodium alginate/titania composite with very good performance for the removal of dye from colored aqueous water. Absalan et al.[12] fabricated an ionic-liquid-modified novel magnetic nanoadsorbent and applied it in a model solution for the removal of Reactive Red 120 and 4-(2-pyridylazo) resorcinol. Xu et al.[13] used a sol–gel method to prepare Fe_3O_4@poly acrylic acid magnetic nanoparticles for the removal of Rhodamine 6G from wastewater. Chowdhury et al.[14] investigated the photocatalytic degradation of methyl orange and methylene blue over a polypyrrole–TiO_2 composite thin film, which was prepared at the air–water interface. Song et al.[15] described the use of TiO_2/poly(fluorine-*co*-thiophene) for the photocatalytic degradation of phenol under the irradiation of visible light. In addition to this, many researchers have investigated the role of polymeric magnetic materials in wastewater treatment.

Several types of natural and synthetic polymers have been modified with magnetic nanoparticles to remove dyes from wastewater.[16–19] However, the synthesis of such a magnetic system included a multistep synthetic route and, hence, was not convenient for use in routine removal processes.

In this context, we designed single-step, surface-modified superparamagnetic iron oxide nanoparticles for the removal of malachite green (MG) dyes. Here, we proposed amine-functionalized

© 2014 Wiley Periodicals, Inc.

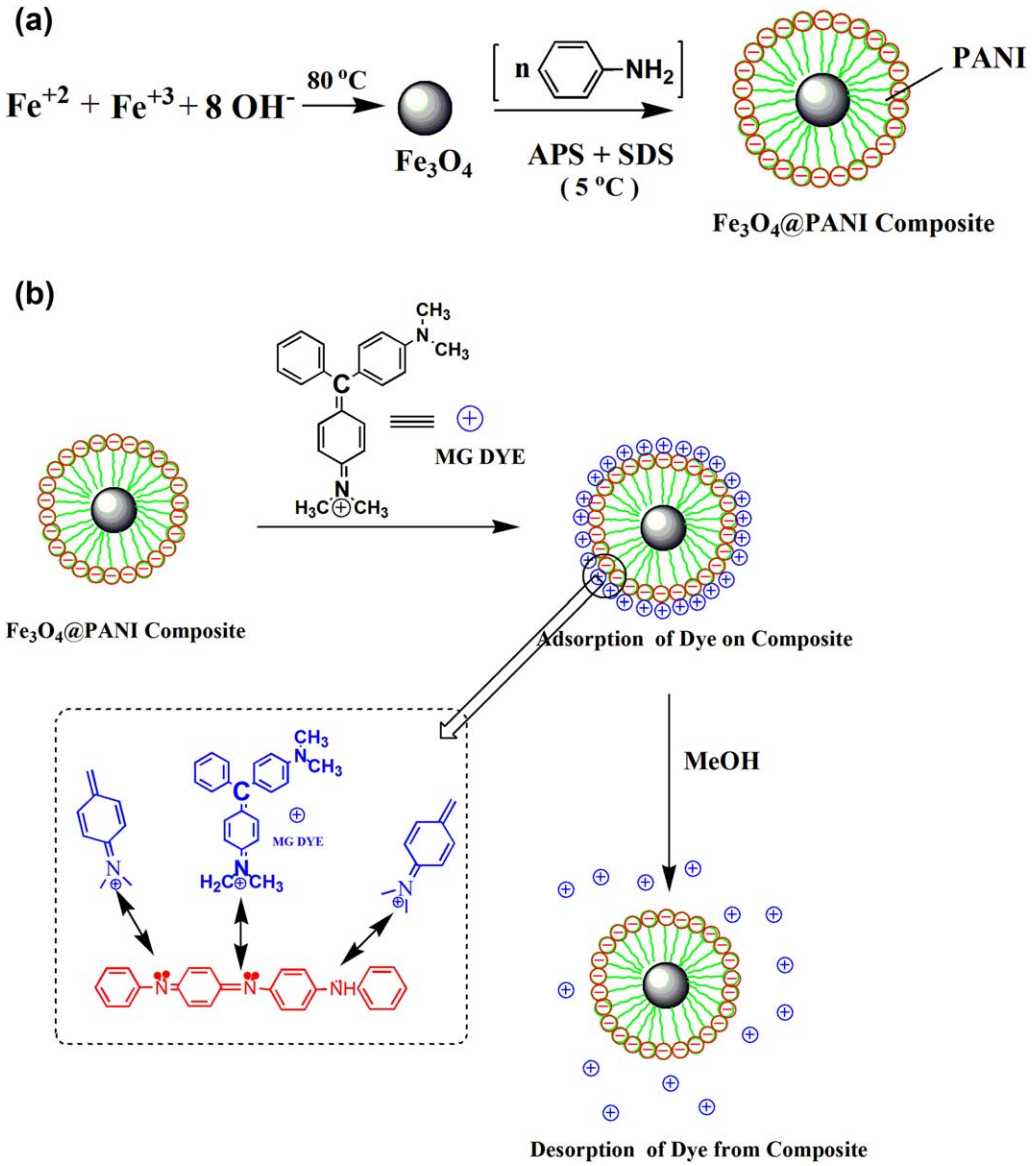

Figure 1. (a) Schematic presentation of the synthesis and functionalization of the Fe_3O_4 nanoparticles. (b) Adsorption and desorption mechanism of MG from the nanocomposites. [Color figure can be viewed in the online issue, which is available at www.interscience.wiley.com.]

magnetite nanoparticles with polyaniline (PANI) as a ligand for the removal of dye molecules. Recently, PANI has attracted much attention because of its several unique advantages; these include its ease of preparation, good environmental stability, ability to be used as a good surface stabilizer, enhanced conductivity, high solubility in various solvents, suitability for making composites with different types of binders, and diverse color changes corresponding to its oxidation levels.[20–22] So, PANI is frequently used for the removal of dye from contaminated wastewater. For instance, a series of PANI-sensitized TiO_2 composite photocatalysts with different mass ratios of PANI to nano-TiO_2 were prepared, and their photocatalytic activities were investigated by the degradation of methylene blue under visible-light irradiation by Wang et al.[23] Eskizeybek et al.[24] studied the photocatalytic activity of PANI homopolymer and PANI/ZnO nanocomposites by the degradation of methylene blue and MG dyes in an aqueous medium under natural sunlight and UV light irradiation. Xiong et al.[25] synthesized PANI/TiO_2 bilayer microtubes with anodic aluminum oxide as a template in a two-step process and found enhanced photocatalytic activity under sunlight in comparison with bare TiO_2 microtubes. Radoicic et al.[26] successfully synthesized PANI/TiO_2 nanocomposites by the *in situ* oxidative polymerization of aniline in colloidal TiO_2 nanoparticles, and the photocatalytic activities of the PANI/TiO_2 nanocomposites were evaluated with the photocatalytic degradation of Rhodamine B and methylene blue as model compounds.

In this study, we provided a facile approach for the synthesis of polyaniline-coated magnetic iron oxide nanoparticles (Fe_3O_4@-PANI). A PANI coating was used to reduce magnetite agglomeration and develop the imine groups on the magnetic surface; this bound the dye molecules through electrostatic interaction. Here, MG was used as a model cationic dye. The efficiency of

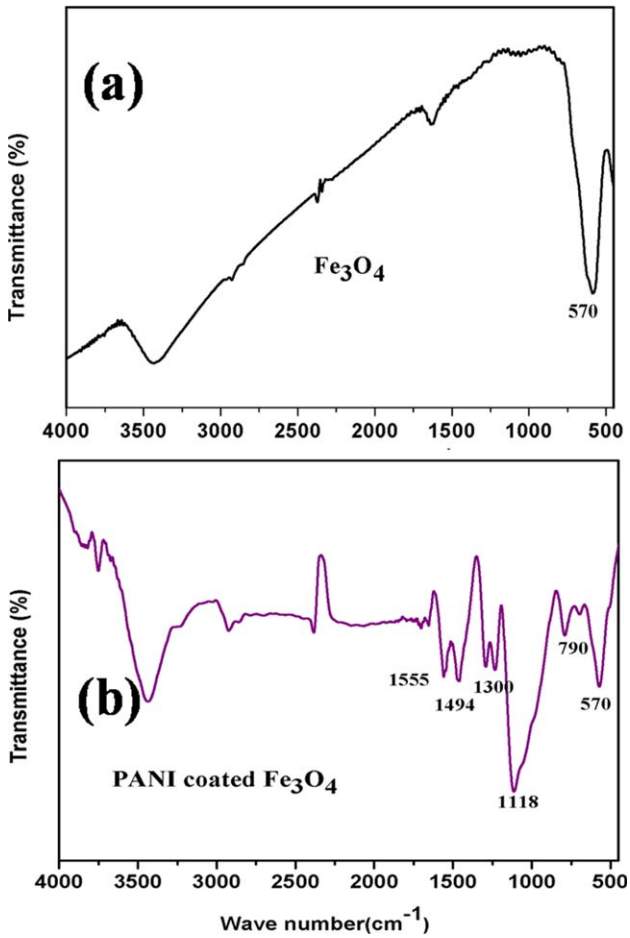

Figure 2. Transmission FTIR spectra of the (a) pure Fe_3O_4 nanoparticles and (b) Fe_3O_4@PANI nanocomposites. [Color figure can be viewed in the online issue, which is available at www.interscience.wiley.com.]

the cationic dye adsorption was evaluated and found to be very efficient. The binding of PANI to the magnetic nanoparticles was confirmed by Fourier transform infrared (FTIR) spectroscopy. The size, structure, and magnetic properties of the resulting magnetic nanoparticles were characterized by transmission electron microscopy (TEM), X-ray diffraction (XRD), and vibrating sample magnetometry. In this article, we describe the first report of the direct formation of a cascading PANI on the surface of magnetite nanoparticles for dye adsorption. To the best of our knowledge, these simply modified magnetic nanoparticles have not been investigated as a tool for dye adsorption.

EXPERIMENTAL

Materials

$FeCl_3$ (anhydrous), $FeSO_4{\cdot}7H_2O$, NH_4OH, ammonium persulfate (APS), and aniline were procured from Merck, India. Sodium dodecyl sulfate (SDS) was obtained from Sigma Aldrich Chemicals. MG was obtained from Loba Chemie, India. All of the chemicals were used as received without further treatment. The water used throughout the experiment was ultrapure Milli-Q water.

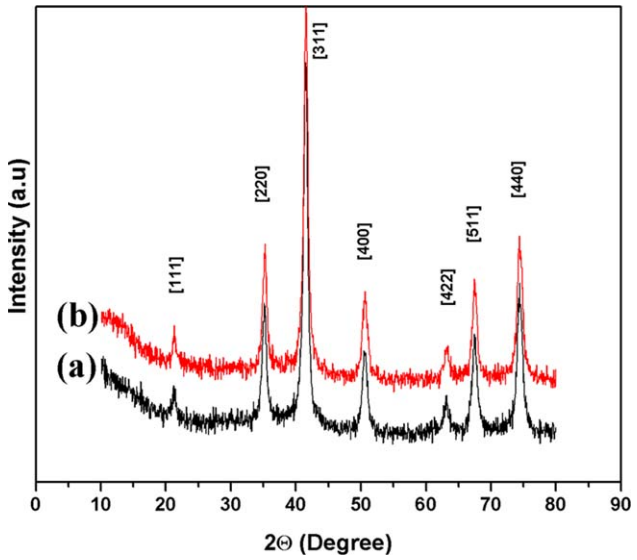

Figure 3. XRD patterns for the (a) pure Fe_3O_4 nanoparticles and (b) Fe_3O_4@PANI nanocomposites [Color figure can be viewed in the online issue, which is available at www.interscience.wiley.com.]

Synthesis and Functionalization of the Magnetite Nanoparticles (Fe_3O_4@PANI)

The steps involved in the synthesis of Fe_3O_4@PANI are illustrated in Figure 1(a). First, superparamagnetic nanosized magnetite particles were prepared according to our previously reported protocol.[27] In a typical recipe, 0.324 g of $FeCl_3$ and 0.274 g of $FeSO_4{\cdot}7H_2O$ were placed in 40 mL of Millipore water under an argon atmosphere. The aqueous ammonia solution (2.5*M*) was dropped into the reaction vessel with violent stirring. Then, the reaction mixture was heated at 80°C, and the pH of the medium was maintained at 10 by the addition of aqueous NH_4OH during the reaction. The obtained magnetite was washed immediately with Millipore water under magnetic separation. After that, the resulting magnetic nanoparticles were dried in a vacuum oven at 50°C. Surface modification was carried out via an *in situ* polymerization technique. A volume of 40 mL of 0.1*M* aniline was placed in a 100-mL round bottom flask and mixed with 0.02*M* SDS. Then, 0.2 g of Fe_3O_4 nanoparticles was added to the solution in an inert atmosphere. The reaction mixture was cooled to 0–5°C. Then, a precooled APS solution (2.0 g in 10 mL) was added slowly to the reaction mixture. The polymerization was allowed to continue for 6 h. A blackish green precipitate was obtained and separated by a permanent magnet. Then, the precipitate was dried in a vacuum oven at 50°C for 1 h and used for adsorption.

Characterization

The presence of surface functional groups was investigated by FTIR spectroscopy (Thermo Nicolet Nexux FTIR model 870). The phase formation and crystallographic state of the uncoated and PANI-functionalized magnetic nanoparticles were determined by XRD with an Expert Pro (Phillips) X-ray diffractometer with Cu Kα. The hydrodynamic size of the aggregate nanocomposites was measured in a Malvern Instruments (United Kingdom). The particle size and microstructure were studied by high-resolution TEM in a

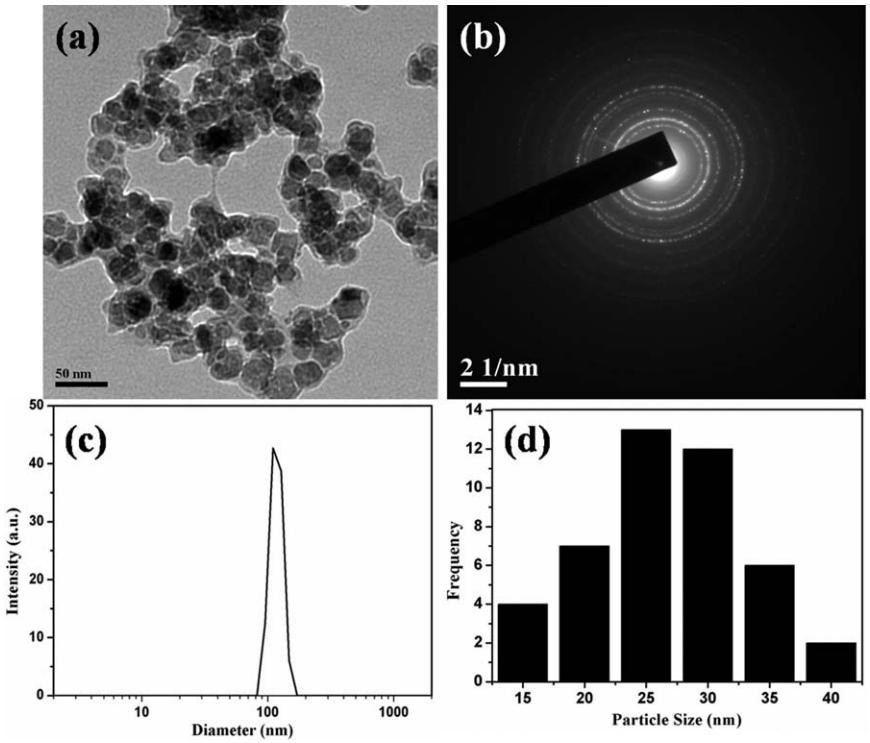

Figure 4. (a) TEM image of Fe_3O_4@PANI, (b) selected area electron diffraction pattern of the same nanoparticles, (c) particle size distribution of the nanoparticles by dynamic light scattering, and (d) particle size distribution of the nanoparticles by TEM.

JEOL 3010 (Japan) operating at 200 keV. Magnetization measurement at room temperature was done by a Lake Shore model 7410 magnetometer.

Dye Adsorption and Desorption Study

The adsorption of MG onto the Fe_3O_4@PANI was carried out in water medium at room temperature and at different pHs. In general, 10 mg of the nanocomposite was added to 10 mL of an MG solution (10 mg/L). After mixing by a vortex for different time intervals, the nanocomposites were removed magnetically from the MG solution. The adsorbed amounts of MG were estimated to measure the change in concentration of the MG in solution by the spectrophotometric method at 617 nm (Hitachi U-3000 ultraviolet–visible spectrophotometer). After several minutes of mixing and the removal of the nanocomposites, the concentration of MG in the liquid solution was measured to estimate the amount of MG desorbed.

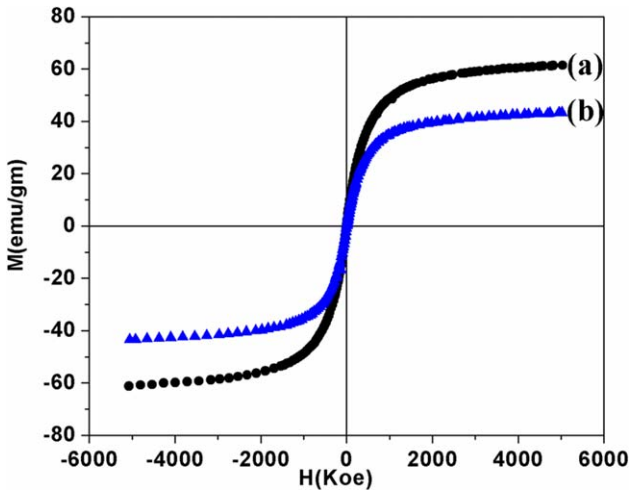

Figure 5. Magnetization curves of the (a) pure Fe_3O_4 and (b) Fe_3O_4@-PANI at room temperature. [Color figure can be viewed in the online issue, which is available at www.interscience.wiley.com.]

The percentage dye removal was calculated by the following equation:

$$\text{Adsorption efficiency}(\%) = \frac{C_0 - C_e}{C_0} \times 100\%$$

where C_0 and C_e are the initial and equilibrium liquid-phase concentrations of malachite green (mg/L), respectively. The amount of MG adsorbed onto the adsorbent could be calculated with the mass balance relationship as follows:

$$q_e = \frac{C_0 - C_e}{W} V$$

where q_e is the adsorption capacity at equilibrium (mg/g), W is the weight of the adsorbent (g), and V is the volume of the solution (L).

For the desorption study, dye was recovered from the nanocomposites with a methanol solution containing 4% acetic acid.[28] Here, 10 mg of nanocomposites was placed into 10 mL of the methanol solution.

RESULTS AND DISCUSSION

Fe_3O_4@PANI was synthesized, and a possible mechanism for the adsorption of the dye molecules is shown in Figure 1(b). In the scientific literature, a number of articles have been published

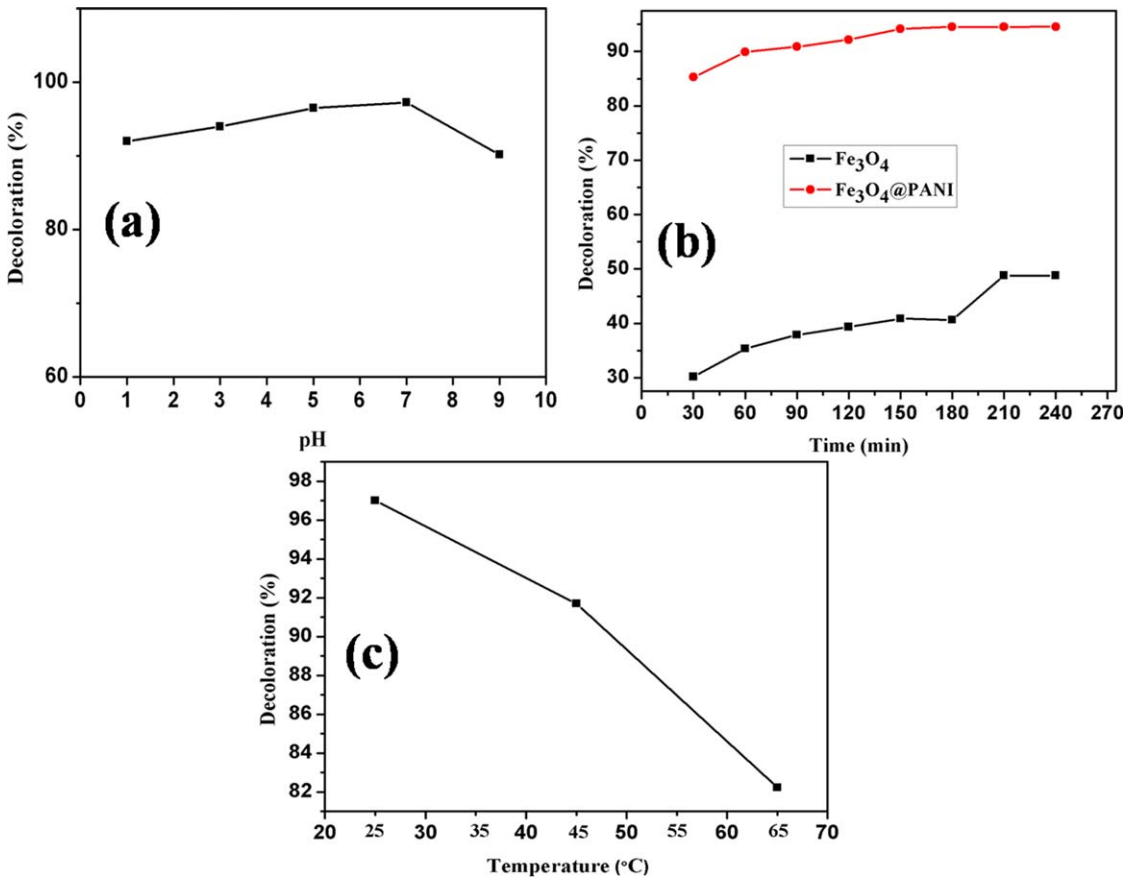

Figure 6. (a) Removal of MG at different pHs when the temperature, dye concentration, and contact time remained the same. (b) Adsorption of MG at different contact time intervals when the other parameters remained the same. (c) Adsorption of MG at different temperatures when the other parameters remained the same. In all cases, the MG volume was 10 mL (10 mg/L), and the adsorbent (Fe_3O_4@PANI) amount was 0.010 g. [Color figure can be viewed in the online issue, which is available at www.interscience.wiley.com.]

that deal with different applications of PANI.[29–31] However, in this study, the PANI-functionalized magnetic nanocomposites were used in cationic dye removal. The main driving force of this adsorption of the MG dye into the Fe_3O_4@PANI was the electrostatic interaction between the basic sites on PANI (amine and imine nitrogens) and the positive part of the cationic dye.

The conjugation of PANI onto the Fe_3O_4 surface was established from the FTIR spectra. A comparison of the FTIR spectrum of the pure magnetic nanoparticles and that of the PANI-modified magnetic nanocomposites is shown in Figure 2. The pure magnetic nanoparticles exhibited a strong band at 570 cm^{-1}, characteristic of the Fe—O vibrations correlated with the magnetic core, and a broad band around 3300 cm^{-1}, which was indicative of the presence of —OH groups on the nanoparticle surface. After the modification of PANI on the nanoparticle surface, a significant decrease in the intensity of the band at 570 cm^{-1} was observed; this indicated the adsorption of PANI on the magnetite surface. The characteristic peaks at 1300, 790, 1494, 1555, and 3450 cm^{-1} were attributed to C—N^+, C—H, C=C, C—N, and N—H bond stretching bands, respectively, for the benzenoid and quinoid rings present in PANI. The presence of these bands confirmed that the magnetic nanoparticles were functionalized with PANI.

The XRD patterns for the bare Fe_3O_4 nanoparticles and Fe_3O_4@PANI nanocomposites are shown in Figure 3. The characteristic peaks at 2θ values of 21.5, 35.2, 41.42, 50.65, 63.33, 67.25, and 74.39° for the pure Fe_3O_4 nanoparticles; these were marked, respectively, by their indices at (111), (220), (311), (400), (422), (511), and (440), which were also observed for the Fe_3O_4@PANI nanocomposites. This revealed that the surface modification of the Fe_3O_4 nanoparticles with PANI did not lead to their phase change. The broadening of the XRD peaks signified the nanocrystalline nature of both the Fe_3O_4 nanoparticles and the Fe_3O_4@PANI nanocomposites.

TEM showed that the ultrafine nanoparticles, with a nearly spherical morphology, organized themselves to form aggregates, as shown in Figure 4(a). Here, PANI was selected as one of the stabilizing agents. The development of the polymerization of aniline emerged as a promising approach for the fabrication of controlled and highly ordered molecular assemblies on nanoparticle surfaces. The thickness of a polymeric layer on the surface of the nanoparticles was of particular interest because of their inherently high surface area. The TEM observation indicated that there was the occurrence of a polymeric layer with a thickness of 6–8 nm on the Fe_3O_4 surface. It was found that the layer could be successfully deposited by polymerization; this led to the formation of core–shell nanocomposites. The selected-area electron diffraction pattern [Figure 4(b)] showed the polycrystalline nature of the embedded magnetite particles. Dynamic

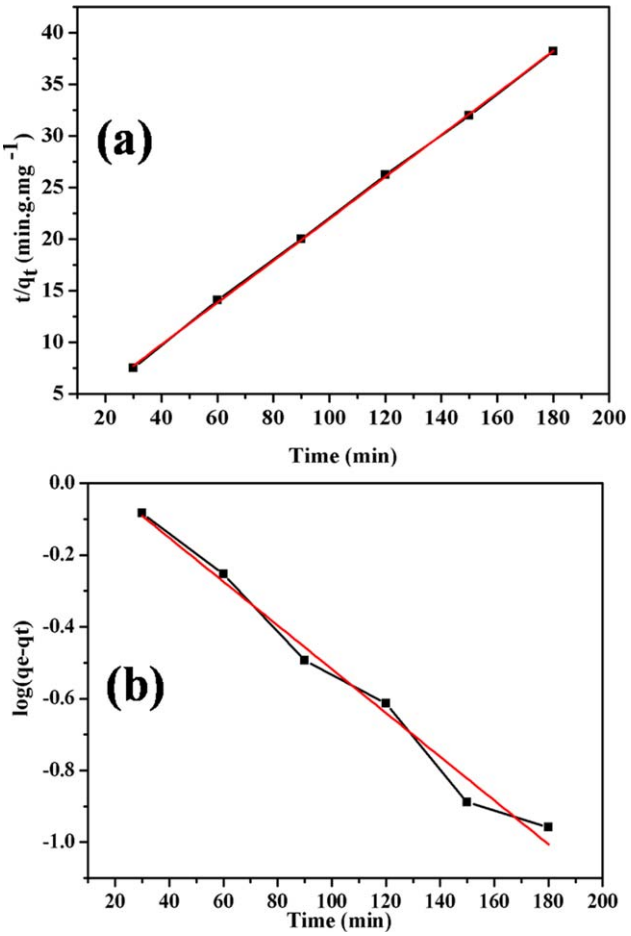

Figure 7. Fitting of the kinetics data to the (a) pseudo-second-order and (b) pseudo-first-order kinetic models. [Color figure can be viewed in the online issue, which is available at www.interscience.wiley.com.]

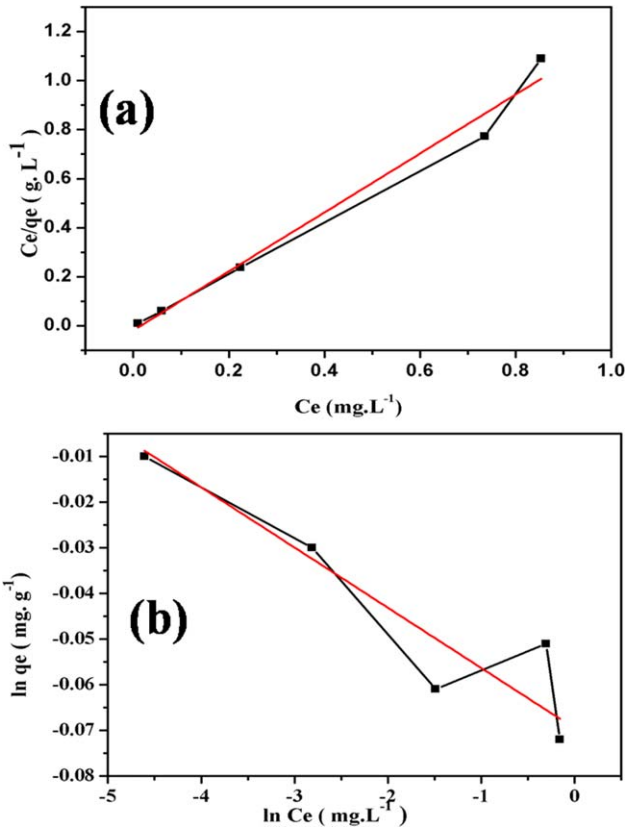

Figure 8. Isotherm plots of the MG adsorption onto the Fe_3O_4@PANI nanocomposites: (a) Langmuir isotherm model and (b) Freundlich isotherm model. [Color figure can be viewed in the online issue, which is available at www.interscience.wiley.com.]

light scattering studies of the PANI-modified magnetic nanocomposites further confirmed the presence of stable, nonaggregated particles with a mean hydrodynamic diameter of 100 ± 10 nm and a polydispersity index less than 0.02, as shown in Figure 4(c). Figure 4(d) shows the frequency plot of the Fe_3O_4@-PANI nanocomposite.

Figure 5 shows the hysteretic magnetization vs magnetic field curves of the bare Fe_3O_4 and Fe_3O_4@PANI nanocomposite at 300 K. The saturation magnetization of the bare Fe_3O_4 nanoparticles was 61.4 emu/g, and that of the Fe_3O_4@PANI nanocomposite was 43.3 emu/g. We observed that the magnetization curves in the two cases demonstrated nearly zero remanence; this proved the existence of the superparamagnetic nature. This reduction in saturation magnetization was partially contributed by the PANI coating. The Fe_3O_4@PANI nanocomposite behaved with active magnetic properties and, therefore, made reuse easy with the help of a permanent magnet.

Effect of pH on the Dye Adsorption

Several researchers have reported the significant role of pH in the adsorption efficacy.[32–34] Here, the effect of the initial pH on the percentage removal of MG through adsorption onto Fe_3O_4@PANI from the dye solution was studied. In that order, experiments were conducted at various pH values, ranging from 1.0 to 9.0 with a 10 mg/L initial dye concentration and 10 mg of nanocomposites (adsorbent) at room temperature for a 240-min equilibrium time, as shown in Figure 6(a). The pH was adjusted with 0.1*M* HCl or 0.1*M* NaOH. The results indicate that the adsorption of cationic dyes onto Fe_3O_4@PANI was fairly pH dependent. The percentage removal of the dye concentration was observed to increase when the pH increased from 1.0 to 7.0. At pH values above 7.0, the percentage removal of

Table I. Kinetic Model Parameters for the Adsorption of MG on Fe_3O_4@PANI at 30°C

		Pseudo first order			Pseudo second order		
C_0 (mg/L)	$q_{e,exp}$ (mg/g)	k_1 (min^{-1})	$q_{e,cal}$ (mg/g)	R^2	k_2 (min^{-1})	$q_{e,cal}$ (mg/g)	R^2
10	4.82	0.0140	1.23	0.9806	0.0250	4.918	0.9996

$q_{e,exp} = q_e$ experimental; $q_{e,cal} = q_e$ calculated.

Table II. Isotherm Model Parameters for the Adsorption of MG on Fe_3O_4@PANI at 30°C

	Langmuir isotherm		Freundlich isotherm	
Temperature	b (L/mg)	R^2	K_f (mg/g)	R^2
300 K	66.13	0.9765	0.85	0.8101

the MG dyes decreased rapidly. PANI exists as emeraldine salt form (protonated quinonoid diimine structures) in a strong acidic medium. This salt form of PANI consisted of a large number of positively charged polaron/bipolaron sites, which underwent electrostatic repulsion with the positive charge of the cationic dye.[35,36] So, the adsorption was less at lower pH, and with increasing pH, the positive charge on Fe_3O_4@PANI decreased. Hence, the electrostatic attraction of the nanocomposites and the cationic dye increased; consequently, the removal of dye increased. A maximum percentage removal of 98% was observed at pH 7.0.

Effect of the Contact Time

Another important parameter that affected the performance of the adsorption process was the contact time between the adsorbent and adsorbate.[37–39] Figure 6(b) illustrates the effect of the contact time on MG removal from an aqueous solution with the Fe_3O_4@PANI nanocomposites. The adsorption started immediately within 5 min just after the addition of an adsorbent to the adsorbate. The percentage adsorption increased with increasing contact time for any initial dye concentration and attained equilibrium within 4 h. These experimental results indicate that the rate of removal of dye from the aqueous solution increased with increasing adsorption time. Almost 85% of the dye was removed within 30 min, but the majority of the dye removal occurred at 210–240 min. The contact of the cationic dye with Fe_3O_4@PANI increased with time, and this might have been the predominant reason for the increasing adsorption. When bare Fe_3O_4 as an adsorbent was used in the 10 mg/L dye solution, the percentage dye removal increased but at a lower percentage. However, when these nanoparticles were functionalized with PANI, the removal reached almost 95% at 4 h.

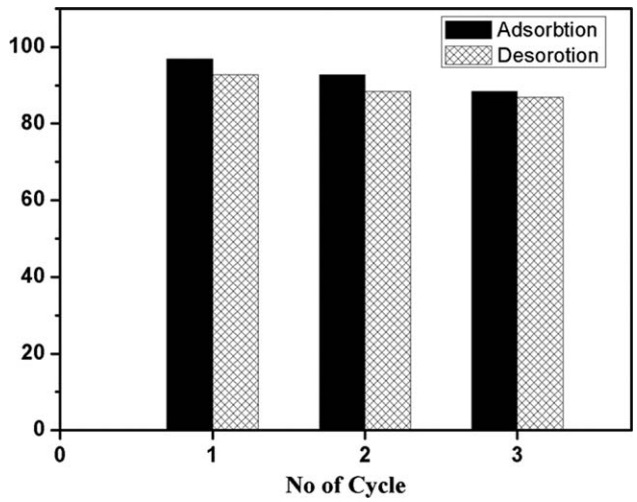

Figure 9. Reusability of the Fe_3O_4@PANI nanocomposites for the removal of MG.

Effect of the Temperature

It is well known that the temperature plays an important role in the adsorption process.[40–42] So, the effect of the temperature for the removal of MG from the Fe_3O_4@PANI nanocomposite was studied at different temperatures, namely, 298, 318, and 338 K, under the process parameters, as shown in Figure 6(c). As the temperature increased, the removal efficiency of the dye decreased. This indicates that this adsorption is exothermic in nature. As the temperature increases mobility of dye molecule increases and consequently less adsorption takes place at higher temperature. In addition with increasing in temperature, viscosity of the solution decreases and consequently diffusion process of dye increases.

Adsorption Kinetics

Several models were available to investigate the adsorption mechanism on the basis of experimental data. The pseudo-first-order and pseudo-second-order reaction rate equations were the most commonly applied models among them.[42] Here, the pseudo-first-order and pseudo-second-order kinetic models were also applied to fit the experimental data obtained from the batch experiments of the adsorption of the dye onto the Fe_3O_4@PANI adsorbent, as shown in Figure 7. The Lagergren pseudo-first-order and pseudo-second-order kinetic models are expressed as follows:

$$\ln(q_e - q_t) = \ln q_e - k_1 t$$

and

$$\frac{t}{q_t} = \frac{1}{k_2 q_e^2} + \frac{t}{q_e}$$

where k_1 and k_2 are constants of the adsorption rate and q_t is the adsorption capacity at time t. The correlation coefficient (R^2) values and rate constant of two models suggested that the adsorption of MG onto Fe_3O_4 followed the pseudo-second-order mechanism. From Table I, it is also clear that for pseudo-second-order mechanism, q_e experimental was close to q_e calculated, but it showed a broad difference from the pseudo-first-order mechanism. So the adsorption of MG on Fe_3O_4@PANI followed pseudo-second-order kinetics. In addition to this, it was dependent on the concentration of the dye on the surface of the functionalized nanocomposites.

Adsorption Isotherm

The adsorption isotherm showed how the adsorbate molecules were distributed between the liquid phase and solid phase. We used the Langmuir and Freundlich isotherm models to describe the experimental data, as shown in Figure 8. The Langmuir isotherm [Figure 8(a)] was valid for monolayer sorption because of the homogeneous surface of the finite number of identical sites. On the other hand, the Freundlich isotherm [Figure 8(b)] assumes that the uptake of dye molecules occurred on a heterogeneous surface by multilayer sorption. The linear form of the Langmuir isotherm is given by the following equation:

$$\frac{C_e}{q_e} = \frac{1}{bQ_0} + \frac{C_e}{Q_0}$$

where Q_0 is the Langmuir constant (mg/g), which represents the monolayer adsorption capacity, and b is the Langmuir equilibrium constant was related to the heat of adsorption (L/mg). The linear plot of C_e/q_e against C_e for the Langmuir isotherm and the parameters b and R^2 are listed in Table II. The essential feature of the Langmuir isotherm could be expressed in terms of a dimensionless factor called the *separation factor* (R_L), which is defined by following equation:

$$R_L = \frac{1}{1 + bC_0}$$

The value of R_L indicates the shape of the isotherm to be either unfavorable ($R_L > 1$), linear ($R_L = 1$), irreversible ($R_L = 0$), or favorable ($0 < R_L < 1$).

The Freundlich isotherm assumes that the adsorption of dye on a heterogeneous surface takes place by multilayer sorption, and it can be presented in the following form.[43]

$$\ln q_e = \ln K_f + \frac{1}{n \ln C_e}$$

where K_f (mg/g) and n are Freundlich constants related to the capacity of sorption and the favorability of sorption, respectively. The figure represents the linear plots of ln q_e versus ln C_e for the Freundlich isotherm and the parameter R^2 are listed in the table (inset). From the R^2 value of the tabulated data, we concluded that it followed the Langmuir adsorption isotherm.

Dye Desorption Study

The reusability of the Fe_3O_4@PANI nanocomposites were further investigated by the separation of the nanocomposites from methanol solution with an external magnet. Because of charge competition, the dye was released to methanol. The nanocomposites were collected magnetically from the methanol. The percentage recovery was about 95%, as shown in Figure 9, depending on the amount of nanocomposite used for dye removal purposes. The magnetic nanocomposites were washed with 10 mL of deionized water and reused the next time.[44]

CONCLUSIONS

In this study, Fe_3O_4 nanoparticles surface-modified by PANI were synthesized and tested as a novel adsorbent for the removal of MG, a model cationic dye. The effect of the pH, contact time, and initial dye concentration on the removal of dye was investigated separately through batch experiments. The results indicate that the synthesized adsorbent effectively removed high concentrations of cationic model dye in a short contact time. Isotherm modeling revealed that the Langmuir equation could better describe the adsorption of MG onto the Fe_3O_4@PANI compared to other models. Kinetic data were appropriately fitted with the pseudo-second-order adsorption rates. These PANI-modified magnetic nanocomposites also exhibited a high adsorption efficiency toward the other organic pollutants, such as methyl orange, crystal violet, and neutral red in aqueous solution and could be easily recycled.

REFERENCES

1. Kabra, A. N.; Khandare, R. V.; Govindwar, S. P. *Water Res.* **2013**, *47*, 1035.
2. Ai, L.; Zhang, C.; Wang, Y.; Li, M.; Meng, L.; Jiang, J. *J. Hazard. Mater.* **2011**, *198*, 282.
3. Pandit; P., Basu; S. *Ind. Eng. Chem. Res.* **2004**, *43*, 7861.
4. Kameda, M.; Seki, H.; Makoshi, T.; Amao, Y.; Nakakita, K. *Sens. Actuators B* **2012**, *171*, 343.
5. Chen, C. Y.; Chang, J. C.; Chen, A. H. *J. Hazard. Mater.* **2011**, *185*, 430.
6. Saha, B.; Das, S.; Saikia, J.; Das, G. *J. Phys. Chem. C.* **2011**, *115*, 8024.
7. Gupta, V. K.; Suhas, J. *Environ. Manage.* **2009**, *90*, 2313.
8. Salehi, R.; Arami, M.; Mahmoodi, N. M. *Colloids Surfaces B* **2010**, *80*, 86.
9. Mahmoodi, N. M.; Bashiri, M.; Moeen, S. *J. Mater. Res. Bull.* **2012**, *47*, 4403.
10. Mahmoodi, N. M.; Najafi, F. *Mater. Res. Bull.* **2012**, *47*, 1800.
11. Mahmoodi, N. M.; Hayati, B.; Arami, M.; Bahrami, H. *Desalination* **2011**, *275*, 93.
12. Absalan, G.; Asadi, M.; Kamran, S.; Sheikhian, L.; Goltz, D. M. *J. Hazard. Mater.* **2011**, *192*, 476.
13. Xu, Y. Y.; Zhou, M.; Geng, H. J.; Hao, J. J.; Ou, Q. Q.; Qi, S. D.; Chen, H. L.; Chen, X. G. *Appl. Surf. Sci.* **2012**, *258*, 3897.
14. Chowdhury, D.; Paul, A.; Chattopadhyay, A. *Langmuir* **2005**, *21*, 4123.
15. Song, L.; Qio, R.; Mo, Y.; Jhang, D.; Wei, H.; Xiong, Y. *Catal. Commun.* **2007**, *8*, 429.
16. Travlou, N. A.; Kyzas, G. Z.; Lazaridis, N. K.; Deliyanni, E. A. *Langmuir* **2013**, *29*, 1657.
17. Debrassi, A.; Correa, A. F.; Baccarin, T.; Nedelko, N.; Waniewska, A. S.; Sobczak, K.; Dłuzewski, P.; Greneche, J. M.; Rodrigues, C. A. *Chem. Eng. J.* **2012**, *183*, 284.
18. Zhu, H. Y.; Jiang, R.; Xiao, L.; Li, W. *J. Hazard. Mater.* **2010**, *179*, 251.
19. Kangwansupamonkon, W.; Jitbunpot, W.; Kiatkamjornwong, S. *Polym. Eng. Sci.* **2010**, *95*, 1894.
20. Ayad, M. M.; Nasr, A. A. E. *J. Phys. Chem. C* **2010**, *114*, 14377.
21. Mahanta, D.; Madras, G.; Radhakrishnan, S.; Patil, S. *J. Phys. Chem. C* **2009**, *113*, 2293.
22. Ayad, M.; Jaghlol, S. *Chem. Eng. J.* **2012**, *204*, 79.
23. Wang, F.; Min, S.; Han, Y.; Feng, L. *Superlattices Microstruct.* **2010**, *48*, 170.
24. Eskizeybek, V.; Sari, F.; Gulce, H.; Gulce, A.; Avci, A. *Appl. Catal. B* **2012**, *119*, 197.
25. Xiong, S.; Wang, Q.; Xia, H. *Synth. Met.* **2004**, *146*, 37.
26. Radoicic, M.; Saponjic, Z.; Jankovic, I. A.; Marjanovic, G. C.; Ahrenkiel, S. P.; Comor, M. I. *Appl. Catal. B.* **2013**, *136*, 133.

27. Sahu, S K.; Chakrabarty, A.; Bhattacharya, D.; Ghosh, S K.; Pramanik, P. *J. Nanopart. Res.* **2010**, *13*, 2475.
28. Ge, F.; Ye, H.; Li, M. M.; Zhao, B. X. *Chem. Eng. J.* **2012**, *198*, 11.
29. Ahn, D.; Koo, Y. M.; Kim, M. G.; Shin, N.; Park, J.; Eom, J.; Cho, J.; Shin, T. J. *J. Phys. Chem. C* **2010**, *114*, 3675.
30. Prathap, M. U. A.; Chaurasia, A. K.; Sawant, S. N.; Apte, S. K. *Anal. Chem.* **2012**, *84*, 6672.
31. Ince, A.; Bayramoglu, G.; Karagoz, B.; Altintas, B.; Bicak, N. *Chem. Eng. J.* **2012**, *189*, 404.
32. Piccin, J. S.; Dotto, G. L.; Vieira, M. L. G.; Pinto, L. A. A. *J. Chem. Eng. Data* **2011**, *56*, 3759.
33. Fu, F.; Gao, Z.; Gao, L.; Li, D. *Ind. Eng. Chem. Res.* **2011**, *50*, 9712.
34. Sharma, P.; Das, M. R. *J. Chem. Eng. Data* **2013**, *58*, 151.
35. Janki, V.; Oh, B. T.; Vijayaraghavan, K.; Kim, J. W.; Kim, S. A.; Ramasamy, A. K.; Kanan, S. K. *Carbohydr. Polym.* **2012**, *88*, 1002.
36. Salem, M. A. *React. Funct. Polym.* **2012**, *70*, 707.
37. He, C.; Hu, X. *Ind. Eng. Chem. Res.* **2011**, *50*, 14070.
38. Roy, A.; Chakraborty, S.; Kundu, S. P.; Adhikari, B.; Majumder, S. B. *Ind. Eng. Chem. Res.* **2012**, *51*, 12095.
39. Peic, A.; Staff, D.; Risbridger, T.; Menges, B.; Peter, L. M.; Walker, A. B.; Cameron, P. J. *J. Phys. Chem. C* **2011**, *115*, 613.
40. Al-Degs, Y. S.; El-Barghouthi, M. I.; El-Sheikh, A. H.; Walker, G. M. *Dyes Pigments* **2008**, *77*, 16.
41. Pal, S.; Ghorai, S.; Das, C.; Samrat, S.; Ghosh, A.; Panda, A. B. *Ind. Eng. Chem. Res.* **2012**, *51*, 15546.
42. Bulut, E.; Ozacar, M.; Sengil, I. A. *Micropor. Mesopor. Mater.* **2008**, *115*, 234.
43. Zhou, L.; Jin, J.; Liu, Z.; Liang, X.; Shang, C. *J. Hazard. Mater.* **2011**, *185*, 1045.
44. Afkhami, A.; Tehrani, M. S.; Bagheri, H. *Desalination* **2010**, *263*, 240.